Journal of Molecular Catalysis A: Chemical 327 (2010) 63–72

Contents lists available at ScienceDirect

Journal of Molecular Catalysis A: Chemical

journal homepage: www.elsevier.com/locate/molcata

Study of the phenol methylation mechanism on zeolites HBEA, HZSM5 and HMCM22

M.E. Sad, C.L. Padró, C.R. Apesteguía*

Catalysis Science and Engineering Research Group (GICIC), Instituto de Investigaciones en Catálisis y Petroquímica-INCAPE-(UNL-CONICET), Santiago del Estero 2654, (3000) Santa Fe, Argentina

ARTICLE INFO

Article history:
Received 13 April 2010
Received in revised form 19 May 2010
Accepted 20 May 2010
Available online 27 May 2010

Keywords:
Phenol methylation
Alkylation
Acid zeolites
Cresols
Anisole

ABSTRACT

The mechanism of gas-phase alkylation of phenol with methanol was studied on zeolites HBEA, HZSM5 and HMCM22. The nature, density and strength of the acid sites were determined by temperature-programmed desorption of NH_3 and FTIR spectroscopy of adsorbed pyridine. In all the cases, anisole, *o*-cresol and *p*-cresol were the primary products, but the initial product distribution greatly depended on the zeolite pore structure and surface acid properties. The complete reaction network was established by investigating the formation of secondary products (xylenols, methylanisoles, *m*-cresol) via the reactions of primary products with phenol and methanol. On HBEA, phenol was alkylated to primary and secondary products without significant diffusional restraints and the yield to dialkylated products increased when phenol conversion was increased. *o*-Cresol was consecutively alkylated to 2,4- and 2,6-xylenols (*C*-alkylation), and 2-methylanisole (*O*-alkylation). Anisole reacted with phenol to yield *o*- and *p*-cresol isomers, and with methanol to form methylanisoles. Selectivities to primary products on HZSM5 were similar to those determined on HBEA, but the formation of bulky intermediates leading to dialkylated compounds was hampered because of diffusional constraints. The alkylation of phenol with anisole to yield cresol isomers was completely suppressed on HZSM5. The particular pore structure of zeolite HMCM22 promoted the selective formation of *p*-cresol among the primary products of phenol methylation and drastically suppressed the consecutive reactions forming secondary products. In contrast, isomerization reactions between monoalkylated products were promoted on zeolite HMCM22 because of its high concentration of strong Brønsted acid sites. The activity decay on stream was significant on the three zeolites, probably because of the formation of coke intermediates via both anisole dealkylation and methanol dehydration reactions.

1. Introduction

The gas-phase methylation of phenol is an important industrial reaction that forms valuable chemicals such as cresols, anisole, and polyalkylated phenols. For example, cresol isomers are widely used for the synthesis of pharmaceuticals, agrochemicals, herbicides and dyes, while 2,6-xylenol is the monomer of several polymer and plastic applications [1–3]. The catalyst selectivity to *O*-alkylated and *C*-alkylated products depends on the active site nature (basic or acid sites), catalyst pore structure and phenol conversion level. Solid bases, in particular MgO, form selectively *ortho*-*C*-alkylated products, namely *o*-cresol and 2,6-xylenol, at temperatures between 673 and 773 K [4,5]. In contrast, solid acids such as silica-alumina, Nafion-H resin, HPA/SiO_2, and zeolites HBEA and HY, convert phenol to a mixture of anisole, cresols, xylenols and methylanisoles, at relatively low temperatures (473–523 K) [6–12]. In general, catalysts containing predominantly strong Brønsted acid sites favor the *O*-alkylation of phenol relative to *C*-alkylation; for example, ultrastable HY zeolite, Nafion-H resin, and HPA/SiO_2 produce anisole/cresols ratios between 2 and 9 [9,10,13]. On the contrary, zeolites containing similar amounts of Lewis and Brønsted acid sites (HBEA, HY) and Lewis solid acids (SiO_2–Al_2O_3) promote preferentially the *C*-alkylation of phenol [6,12–14]. Regarding the *para*/*ortho* selectivity for *C*-alkylated products, *o*-cresol is always formed preferentially in comparison to *p*-cresol on amorphous acid catalysts or wide pore zeolites such as HBEA, HY, and H-mordenites [8,10,13,15]. However, acid zeolites of narrow channels such as zeolite HMCM22 promote the selective formation of *p*-cresol [16,17]. All these studies show that the reaction mechanism, and therefore the product distribution, of phenol methylation greatly depend on the nature and strength of surface acid sites and also on the catalyst pore microstructure. Nevertheless, efforts devoted to elucidate the exact requirements of density, nature and strength of surface acid sites for selectively improving the reaction path-

* Corresponding author.
E-mail address: capesteg@fiq.unl.edu.ar (C.R. Apesteguía).
URL: http://www.fiq.unl.edu.ar/gicic (C.R. Apesteguía).

1381-1169/$ – see front matter © 2010 Elsevier B.V. All rights reserved.
doi:10.1016/j.molcata.2010.05.014

ways leading from phenol to a desired alkylated product are still needed.

Recently, we investigated the gas-phase methylation of phenol on SiO_2–Al_2O_3 and zeolites HBEA, HZSM5 and HMCM22 [17]. Our goal was to explore the possibility of drastically improving the reaction selectivity to obtain *p*-cresol. The development of a novel process using solid catalysts is a highly desirable technological target for the *p*-cresol synthesis because the current commercial process involves the oxidation of toluene via sulfonation with sulfuric acid and entails concerns related to corrosion and disposal of spent base materials [1]. We observed that the *para*-selectivity was dramatically increased by using zeolite HMCM22. In fact, the *p*-cresol yield and the *para*-/*ortho*-cresol ratio on HMCM22 for 93% phenol conversion were about 58% and 3.4, respectively, the highest values reported up to now for the *p*-cresol formation from methylation of phenol. In this paper, we have extended these studies with the aim of ascertaining the complete reaction network of phenol methylation on zeolites HBEA, HZSM5 and HMCM22. We first identified primary and secondary pathways involved in the reaction mechanism by modifying the contact time. Then, we investigated the formation of secondary products (xylenols, methylanisoles, *m*-cresol) via the reactions of primary products with phenol or methanol. Specifically, we studied the *o*-cresol methylation, the alkylation of phenol with anisole, the anisole/methanol reactions and the pure anisole conversion reactions. Results allowed us to establish and explain the differences in the reaction mechanism of phenol methylation on zeolites HBEA, HZSM5 and HMCM22. Reaction pathways are mainly influenced by the zeolite pore microstructure but the Lewis/Brønsted acid sites ratio and the strength of Brønsted sites also play a significant role.

2. Experimental

2.1. Catalyst preparation

Commercial zeolites HZSM5 (Zeocat Pentasil PZ-2/54) and HBEA (Zeocat PB) were calcined in air at 723 K. Zeolite HMCM22 was synthesized according to Ref. [18], by using sodium aluminate (Alfa Aesar, Technical Grade), silica (Aerosil Degussa 380), sodium hydroxide (Merck, >99%), hexamethyleneimine (Aldrich, 99%) and deionized water as reagents. The molar composition of the synthesis gel was $SiO_2/Al_2O_3 = 30$, $OH/SiO_2 = 0.18$, hexamethyleneimine/$SiO_2 = 0.35$ and $H_2O/SiO_2 = 45$. The gel was transferred to a Teflon lined stainless steel autoclave, rotated at 50 rpm, and heated to 423 K in an oven for 7–10 days. After crystallization, the solid was washed with deionized water, centrifugated, dried at 373 K, and finally heated first in N_2 and then in air at 773 K for 15 h.

2.2. Catalyst characterization

The crystalline structure of the samples was determined by X-ray diffraction (XRD) in the range of $2\theta = 2$–45°, using a Shimadzu XD-D1 diffractometer and Ni-filtered Cu Kα radiation ($\lambda = 1.540$ Å). BET surface areas (S_g) were measured by N_2 physisorption at its boiling point in a Micromeritics Accusorb 2100 E sorptometer. Prior to N_2 physisorption, samples were degassed for 3 h at 523 K. Elemental compositions were measured using atomic absorption spectroscopy.

Acid site densities were determined by temperature-programmed desorption (TPD) of NH_3 preadsorbed at 373 K. Samples (100 mg) were treated in He (60 cm^3/min) at 723 K for 2 h and then exposed to a 1% NH_3/He stream for 40 min at 373 K. Weakly adsorbed NH_3 was removed by flushing with He at 373 K during 2 h. Temperature was then increased at a rate of 10 K/min and the NH_3 concentration in the effluent was measured by mass spectrometry in a Baltzers Omnistar unit.

The nature of surface acid sites was determined by infrared spectroscopy (IR) using pyridine as probe molecule and a Shimadzu FTIR-8101M spectrophotometer. The spectral resolution was 4 cm^{-1} and 50 scans were added. Sample wafers were formed by pressing 20–40 mg of the catalyst at 5 ton/cm^2 and transferred to a sample holder made of quartz. An inverted T-shaped Pyrex cell containing the sample pellet was used. The two ends of the short arm of the T were fitted with CaF_2 windows. All the samples were initially outgassed in vacuum at 723 K for 4 h and then a background spectrum was recorded after cooling the sample at room temperature. Spectra were recorded at room temperature, after admission of pyridine, adsorption at room temperature and evacuation at 423 K. Difference spectra were obtained by subtracting the background spectrum recorded previously.

2.3. Catalyst testing

The gas-phase alkylation of phenol (Merck, >99%) with methanol (Merck, 99.8%) was carried out in a fixed bed tubular reactor at 473 K and 101.3 kPa. Samples were sieved to retain particles with 0.35–0.42 mm diameter for catalytic measurements and pretreated in air at 723 K for 2 h before reaction in order to remove H_2O, hydrocarbons, and CO_2. A mixture of methanol (M) and phenol (P) of M/P = 2:1 molar ratio was fed using a syringe pump and vaporized into flowing N_2 to give a N_2/(P + M) molar ratio of 26.8. Standard catalytic tests were conducted at contact times (W/F_P^0) of 56 or 112 g h/mol. Reaction products were analyzed by on-line gas chromatography using an Agilent 6850 chromatograph equipped with a flame ionization detector, temperature programmer and a 30 m Innowax column (inner diameter: 0.32 mm, film thickness: 0.5 μm). Samples were collected every 20 min during 4 h. Main reaction products were cresols (*o*-, *m*- and *p*-cresols), anisole, xylenols (dimethylphenols) and methylanisoles (MA); dimethyl ether produced by methanol dehydration was also detected. Phenol conversion (X_P) was calculated as: $X_P = \Sigma Y_i/(\Sigma Y_i + Y_P)$, where ΣY_i is the molar fraction of products formed from phenol, and Y_P is the outlet molar fraction of phenol. The selectivity to product *i* (S_i, mol of product *i*/mol of phenol reacted) was determined as: $S_i = [Y_i/\Sigma Y_i]$. Yields (η_i, mol of product *i*/mol of phenol fed) were calculated as $\eta_i = S_i X_P$. Additional catalytic tests were performed using the same reactor unit to gain insight on the phenol alkylation mechanism. Specifically, anisole (Merck, >99%) and *o*-cresol (Anedra, >99%) were fed to the reactor together with phenol or methanol at the same operating conditions detailed above for the alkylation of phenol with methanol.

3. Results and discussion

3.1. Catalysts characterization

Zeolites HBEA and HZSM5 were commercial samples while zeolite HMCM22 was synthesized in our laboratory. The positions and intensities of X-ray diffractograms (not shown here) corresponding to both the HMCM22 precursor, i.e. the as-synthesized sample, and calcined zeolite HMCM22 were in good agreement with those published for the synthesis of HMCM22 zeolites [19]. The sample physicochemical properties are shown in Table 1. The Si/Al molar ratio varied between 12.5 (HBEA) and 20.0 (HZSM5). The BET surface area of HBEA (560 m^2/g) was higher than those determined for HMCM22 (400 m^2/g) and HZSM5 (350 m^2/g).

Sample acid properties were probed by TPD of NH_3 preadsorbed at 373 K and by IR spectra of adsorbed pyridine after admission at 298 K and evacuation at 423 K. Fig. 1 shows the NH_3 TPD curves

Table 1
Physicochemical and acid properties of zeolites HBEA, HZSM5 and HMCM22.

Catalyst	Physicochemical properties			Surface acid properties			
	Si/Al	Surface area (m^2/g)	Pore size (Å)	TPD of NH_3 (μmol/m^2)	IR of pyridine		
					L (area/g)[a]	B (area/g)[a]	B/L
HBEA	12.5	560	6.6 × 6.7; 5.6 × 5.6	0.90	272	282	1
HZSM5	20.0	350	5.1 × 5.5; 5.3 × 5.6	2.20	341	337	1
HMCM22	15.0	400	4.0 × 5.5; 4.1 × 5.1	1.18	176	560	3.2

[a] By FTIR of pyridine adsorbed at 298 K and evacuated at 423 K (B: Brønsted sites; L: Lewis sites).

obtained for the zeolites used in this work. The TPD profile of HZSM5 consisted of a peak at about 531 K and a broad band at higher temperatures. Zeolite HMCM22 exhibited a qualitatively similar TPD profile to that of HZSM5, showing two main NH_3 desorption bands centered at about 575 and 750 K, respectively. The TPD curve corresponding to HBEA presented a single asymmetric broad band with a maximum at around 610 K which is consistent with previous results obtained on zeolites HBEA of similar Si/Al ratios [20]. The total amount of desorbed NH_3 (μmol/m^2) was measured by deconvolution and integration of the TPD traces and it was taken as an indication of the total acid site density. The results are reported in Table 1. Zeolite HZSM5 exhibited the highest density of acid sites (2.20 μmol/m^2) in comparison to HMCM22 (1.18 μmol/m^2) and HBEA (0.90 μmol/m^2).

IR spectra obtained after admission of pyridine at 298 K and evacuation at 423 K allowed us to establish the nature of surface acid sites. Fig. 2 shows the IR spectra obtained on zeolites HBEA, HZSM5 and HMCM22. The IR band assignment of the surface species arising from the adsorption of pyridine on acid zeolites has been reported by several authors [21–24]. The band at 1540 cm^{-1} is characteristic of the formation of pyridinium ions on Brønsted acid sites while the band between 1440 and 1460 cm^{-1} arises from coordinatively bonded pyridine on Lewis acid sites. The relative contributions of Lewis and Brønsted acid sites were obtained by deconvolution and integration of the corresponding pyridine absorption bands in Fig. 2. Results are given in Table 1. The amounts of adsorbed pyridine on both Brønsted and Lewis sites of HBEA were significantly lower than those adsorbed on HMCM22 and HZSM5, thereby confirming that HBEA was the least acidic zeolite, as suggested by the NH_3 TPD curves in Fig. 1. The B/L ratios determined on HBEA and HZSM5 evacuated at 423 K were close to one. Zeolite HMCM22 contained the highest concentration of Brønsted acid sites and also the highest B/L ratio (B/L = 3.2). This B/L ratio is consistent with the results reported by other authors showing that zeolites HMCM22 with Si/Al atomic ratios of about 15 contain B/L ratios between 2 and 4.5 [25,26].

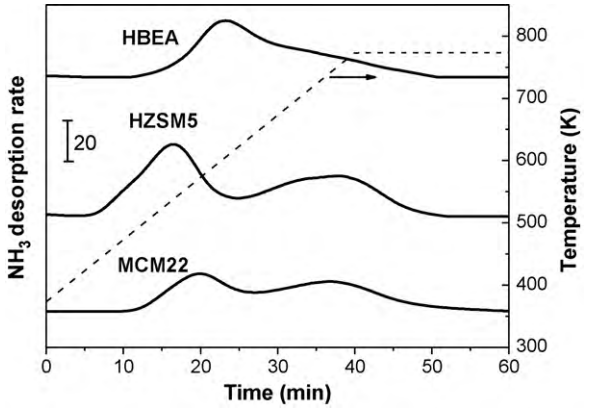

Fig. 1. TPD profiles of NH_3 on zeolites HBEA, HZSM5 and HMCM22. NH_3 adsorption at 373 K, heating rate: 10 K/min.

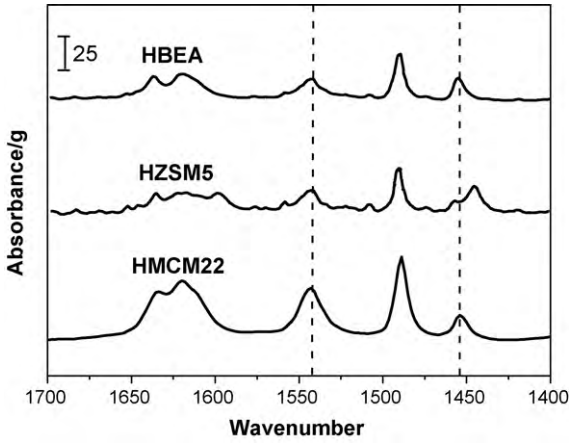

Fig. 2. FTIR spectra after pyridine adsorption at 298 K and evacuation at 423 K. Dotted lines indicate the presence of Lewis (1450 cm^{-1}) and Brønsted (1540 cm^{-1}) acid sites.

3.2. Catalytic tests

3.2.1. Phenol methylation

Fig. 3 shows the evolution of phenol conversion and selectivities as a function of time obtained at 473 K on HZSM5 and typically illustrates the time-on-stream behavior of the catalysts during the reaction. Phenol conversion (X_P) was initially 35% but continuously diminished with the progress of the reaction reaching 8% after 3 h on stream. Similar catalyst activity decay was observed on HBEA and HMCM22 reflecting the in situ deactivation of the samples. Fig. 3 shows that cresols and anisole were the main products on HZSM5. The selectivity to cresols was about 50% and remained approximately constant during the 4-h catalytic test. The selectivity

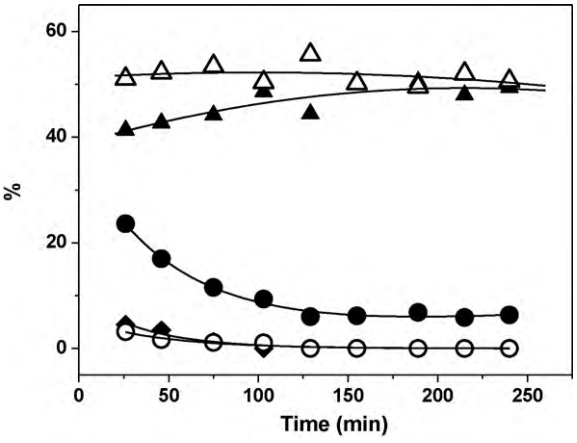

Fig. 3. Methylation of phenol. Phenol conversion (●) and selectivities as a function of time on HZSM5. Selectivities to: cresols (△), anisole (▲), xylenols (♦), and MA (○) (473 K, 101.3 kPa, $W/F_P^0 = 112$ g h/mol, M/P = 2, N_2/(P + M) = 26.8).

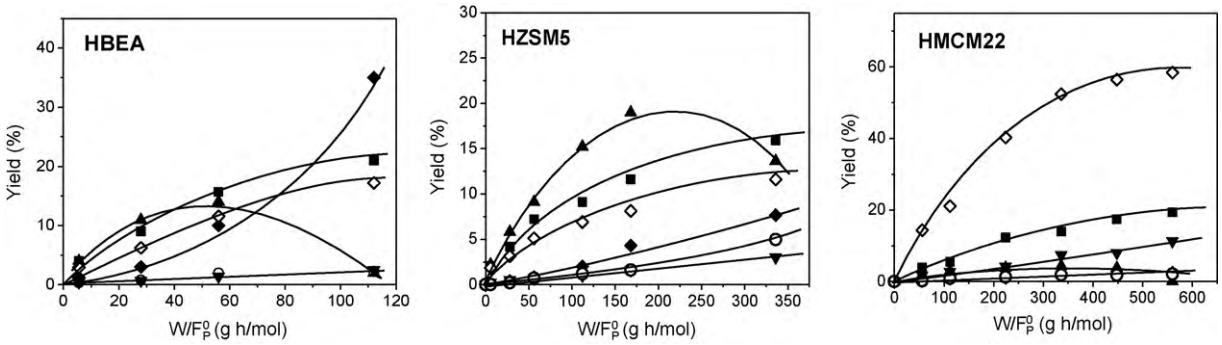

Fig. 4. Methylation of phenol. Yields as a function of contact time on HBEA, HZSM5 and HMCM22. Anisole (▲), *o*-cresol (■), *p*-cresol (◊), *m*-cresol (▼), xylenols (⧫), and MA (○). Operating conditions as in Fig. 3.

to anisole increased at the expense of xylenols and methylanisoles (MA), reaching 50% at the end of the run.

To identify primary and secondary reaction products we investigated the effect of contact time on the product distribution. The deactivation of all the samples, however, required that each data point be obtained on a fresh catalyst and that initial yields be obtained by extrapolating to initial time on stream. The yields at $t = 0$ on zeolites HBEA, HZSM5 and HMCM22 are shown as a function of contact time in Fig. 4. The local slopes of the curves in Fig. 4 give the rate of formation of each product at a specific phenol conversion and residence time. The nonzero initial slopes for anisole, *o*-cresol and *p*-cresol show that they form directly from phenol and are therefore primary products on the three zeolites. The direct attack of methanol to phenol produces anisole by *O*-alkylation, and *o*- and *p*-cresols by *C*-alkylation (Fig. 5). This later result shows that methanol attacks the phenol ring by electrophilic substitution essentially in *ortho* and *para* positions, probably reflecting the electron donor effect of the phenol OH group that increases the electronic density of positions 2, 4, and 6 in the ring. On the other hand, the zero initial slopes observed for *m*-cresol, xylenols and methylanisoles in Fig. 4 for the three zeolites suggest that these compounds are secondary products. Although the methylation of phenol formed the same primary products on zeolites HBEA, HZSM5 and HMCM22 (Fig. 5), the primary product distribution depended on the type of zeolite used. In fact, Fig. 4 shows that zeolite HMCM22 formed mainly *p*-cresol while zeolites HBEA and HZSM5 produced mostly anisole and *o*-cresol (in similar yields).

3.2.2. *Catalytic tests using intermediate reaction products*

In this work we particularly investigated the formation mechanism of secondary products for the phenol methylation reaction with the aim of establishing the complete reaction pathway network occurring on zeolites HBEA, HZSM5 and HMCM22. To achieve this goal, we studied the conversion of primary to secondary products by feeding anisole or *o*-cresol to the reactor, with or without methanol or phenol. Contact times of 27 g h/mol of reactant was used on HBEA and of 112 g h/mol on HZSM5 and HMCM22. Similar initial phenol conversions ($X^0_p \cong 35\%$) are obtained using these contact times values for the phenol methylation reaction.

3.2.2.1. Reactants: o-cresol/methanol mixture. Fig. 6 shows the evolution of conversion and selectivities during the alkylation of *o*-cresol with methanol on zeolite HBEA. Main products were xylenols (2,4- and 2,6-xylenol) and 2-methylanisole which are formed by *C*- and *O*-alkylation of *o*-cresol, respectively (Reaction 1). Minor amounts of *p*- and *m*-cresol formed from *o*-cresol isomerization were also observed (Reaction 2). Qualitatively, similar results were reported by Marczewski et al. [9] on ultrastable HY zeo-

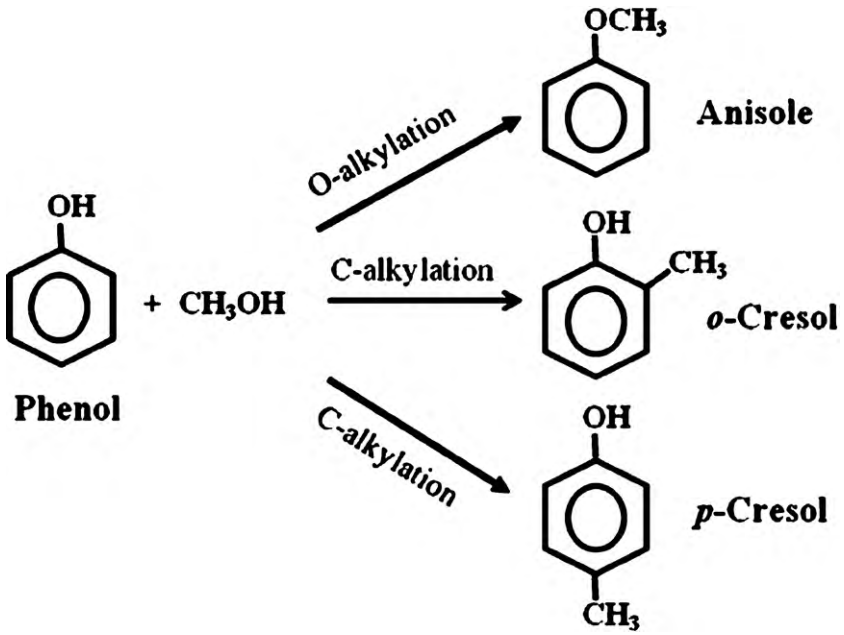

Fig. 5. Methylation of phenol. Formation of primary products.

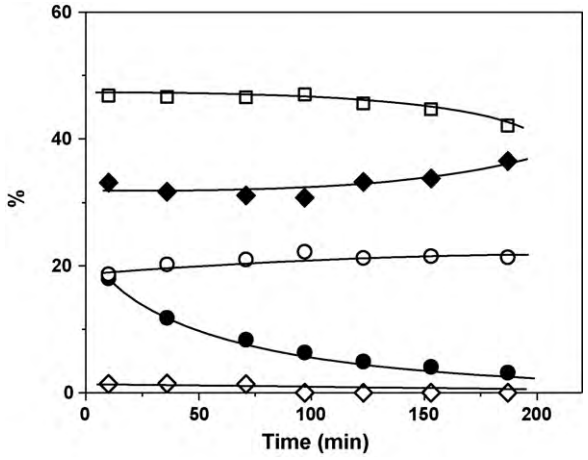

Fig. 6. Reactants: *o*-cresol/methanol mixture. *o*-Cresol conversion (●) and selectivities on HBEA. Selectivities to: 2,4-xylenol (□), 2,6-xylenol (♦), 2-MA (○), and *p*-cresol (◊) (473 K, 101.3 kPa, $P_{o\text{-cresol}} = 1.013$ kPa, methanol/*o*-cresol = 5, $W/F^0_{o\text{-cresol}} = 27$ g h/mol).

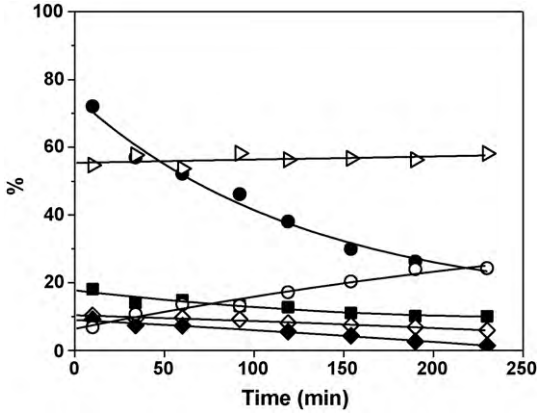

Fig. 7. Reactant: anisole. Anisole conversion (●) and selectivities as a function of time on HBEA. Selectivities to: phenol (▷), *o*-cresol (■), *p*-cresol (◊), xylenols (♦), and MA (○) (473 K, 101.3 kPa, $P_{\text{anisole}} = 1.013$ kPa, $W/F^0_{\text{anisole}} = 27$ g h/mol).

lites. The values of *o*-cresol conversion and selectivities obtained by extrapolating at $t = 0$ the curves of Fig. 6 are given in Table 2. Results obtained on zeolites HZSM5 and HMCM22 are also included in Table 2. *o*-Cresol conversion was four times lower on HZSM5 in comparison to HBEA, in spite that a higher contact time was used for HZSM5 sample.

Reaction 1: *o*-Cresol methylation

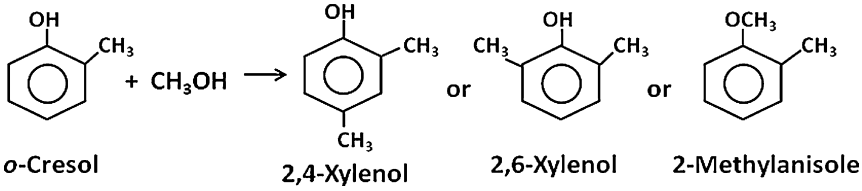

Reaction 2: *o*-Cresol isomerization

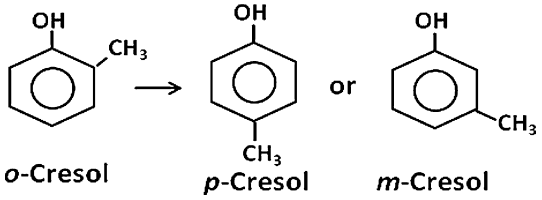

Besides, on HZSM5 the selectivity to 2,4-xylenol ($S_{2,4\text{-xylenol}} = 80\%$) was clearly improved at the expense of 2,6-xylenol. These differences in activity and selectivity observed between HZSM5 and HBEA are explained on the basis of diffusional (lower activity) and shape (lower selectivity to bulky 2,6-xylenol) constraints existing in HZSM5 due to its narrower pore structure (Table 1). In contrast with HBEA and HZSM5, zeolite HMCM22 converted *o*-cresol mainly to *p*-cresol ($S_{p\text{-cresol}} = 46\%$) and also to *m*-cresol ($S_{p\text{-cresol}} = 9\%$). This result shows that zeolite HMCM22 is highly active for promoting isomerization reactions, probably reflecting its high density of Brønsted acid sites (Table 1). On the other hand, *o*-cresol conversion was three times higher on HMCM22 than on HZSM5, in spite that more diffusional constraints are expected in HMCM22 for bulkier molecules because its lower mean pore size. The superior activity obtained on HMCM22 reflects the particular ability of HMCM22 for converting *o*-cresol to *para* and *meta* isomers. In fact, this isomerization reaction is less

Table 2
Catalytic results for *o*-cresol/methanol reactions.

Catalysts	$X_{o\text{-cresol}}$ at $t = 0$ (%)	Selectivity at $t = 0$ (%)				
		p-Cresol	*m*-Cresol	2-MA	2,6-Xylenol	2,4-Xylenol
HBEA	20	2	2	18	33	45
HZSM5	5	1	1	9	9	80
HMCM22	15	46	9	5	10	30

$T = 473$ K, $P = 101.3$ kPa, $P_{o\text{-cresol}} = 1.013$ kPa, and methanol/*o*-cresol = 5.

Table 3
Catalytic results for anisole conversion reactions.

Catalyst	X_{anisole} at $t = 0$ (%)	Selectivity at $t = 0$ (%)					
		Phenol	*o*-Cresol	*m*-Cresol	*p*-Cresol	Xylenols	MA
HBEA	80	55	17	0	10	11	7
HZSM5	31	59	10	1	10	0	20
HMCM22	100	60	8	1	30	0	1

$T = 473$ K, $P = 101.3$ kPa, and $P_{\text{anisole}} = 1.013$ kPa.

affected by diffusional restrictions because it involves the formation of smaller intermediates in comparison to alkylation reactions forming xylenols or methylanisoles. In summary, our results show that the activity and selectivity of *o*-cresol methylation on acid zeolites greatly depend on both the zeolite structure and the density and nature of surface acid sites.

3.2.2.2. Reactant: anisole. Fig. 7 shows the catalytic results obtained when pure anisole was fed to the reactor on zeolite HBEA. Anisole formed mainly phenol and also methylanisoles, *o*-cresol, *p*-cresol and minor amounts of *m*-cresol and xylenols. The selectivity to phenol remained approximately constant while the selectivity to methylanisoles increased at the expense of xylenols and cresol isomers. The initial anisole conversion (80%) decreased to 25% at the end of the 4-h run. The selectivities determined by extrapolating at $t = 0$ the curves of Fig. 7 are shown in Table 3. The catalytic values obtained on HZSM5 and HMCM22 are also included in Table 3. Initial anisole conversions on HBEA and HMCM22 were significantly higher than on HZSM5. The three zeolites formed initially similar amounts of phenol, between 55 and 60%. Phenol may be obtained from anisole either by disproportionation (self-alkylation of anisole) giving also methylanisoles (Reaction 3) or by anisole dealkylation forming phenol and olefins (Reaction 4) [27].

Reaction 3: Anisole disproportionation

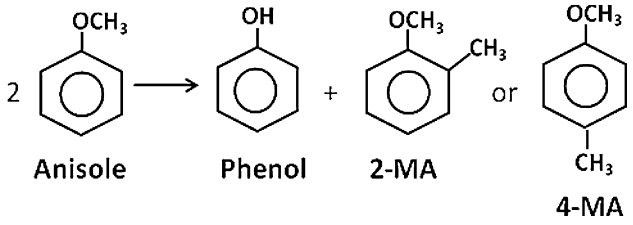

Reaction 4: Anisole dealkylation

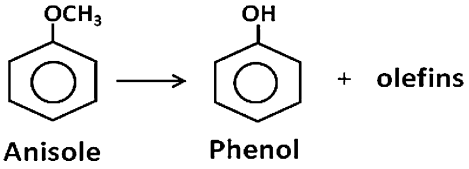

Results in Table 3 show that in all the cases the selectivity to phenol was clearly higher than those to MA thereby indicating that phenol is mainly formed from anisole dealkylation. The presence of heavy olefins among the products was always detected which can explain the significant activity decay observed on stream on all the samples; olefins are well known intermediates for the formation of coke.

Fig. 7 shows that HBEA produced initially about 10% of xylenols, probably by methylanisole rearrangement. In contrast, zeolite HZSM5 did not form xylenols, thereby suggesting that its narrow channels hampered the formation of bulky intermediates involved in xylenol formation. Fig. 7 also shows that on HBEA the selectivity to MA increased at the expense of cresol isomers as anisole conversion decreased with the progress of the reaction. This result suggests that cresols are in part formed from MA dealkylation (Reaction 5) as it has been proposed by Jacobs et al. [27].

Reaction 5: Methylanisole dealkylation

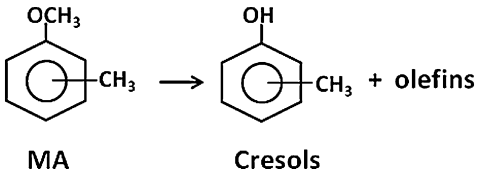

In contrast, Reaction 5 does not take place on HMCM22 because this zeolite did not form MA from anisole (Table 3). Direct anisole isomerization (Reaction 6) formed *o*- and *p*-cresol on the three zeolites, but the selectivity to *p*-cresol was particularly significant on HMCM22 ($S_{p\text{-cresol}} = 30\%$).

Reaction 6: Anisole rearrengement

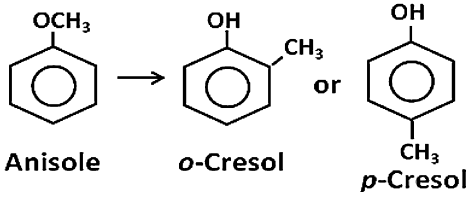

3.2.2.3. Reactants: anisole/phenol mixture. The evolution of anisole conversion and selectivities on HBEA when an anisole/phenol mixture was introduced to the reactor is presented in Fig. 8. In this case, phenol is a reactant but also a product of the reaction, so that the selectivity to phenol (S_P, mol of P produced/mol of anisole reacted) was determined as $(Y_P^{out} - Y_P^{in})/[\sum Yi + (Y_P^{out} - Y_P^{in})]$, where Y_P^{in} and Y_P^{out} are the molar fractions of phenol in the feed and in the products, respectively, and $\sum Yi$ is the molar fraction of products formed from anisole, excepting phenol. Cresols may be formed now via two reaction pathways: (i) intramolecular rearrangement of anisole (Reaction 6) and (ii) alkylation of phenol with anisole (Reaction 7). Regarding this later reaction, previous studies [9,15] have specifically reported that anisole may produce cresols on solid acids by alkylating phenol, in particular by considering that anisole is a more effective alkylating agent than methanol [28].

Reaction 7: Alkylation of phenol with anisole

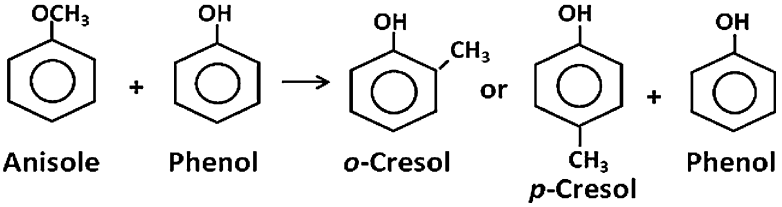

Catalytic results obtained at $t = 0$ on HBEA, HZSM5 and HMCM22 are presented in Table 4. It is observed that on HBEA the selectivity to cresol isomers ($S_{cresols} = 72\%$) increased in comparison with the values obtained by feeding pure anisole (Table 3, $S_{cresols} = 27\%$), thereby showing that phenol is effectively alkylated by anisole. Besides, formation of xylenols and methylanisoles was practically suppressed on HBEA, probably because the presence of phenol among the reactants hinders the anisole disproportionation reaction (Reaction 3). In contrast, the selectivities to cresol isomers on HZSM5 and HMCM22 (Table 4) were slightly lower than those obtained using pure anisole as reactant (Table 3). This result strongly suggests that cresols are essentially formed from direct anisole isomerization (Reaction 6) and not via phenol alkylation (Reaction 7) when an

Table 4
Catalytic results for anisole/phenol reactions.

Sample	$X_{anisole}$ at $t = 0$ (%)	Selectivity at $t = 0$ (%)					
		Phenol	*o*-Cresol	*m*-Cresol	*p*-Cresol	Xylenols	MA
HBEA	61	24	45	3	24	0	4
HZSM5	31	85	6	1	6	0	2
HMCM22	88	69	5	3	23	0	0

$T = 473$ K, $P = 101.3$ kPa, $P_{anisole} = 1.013$ kPa, and phenol/anisole = 3.

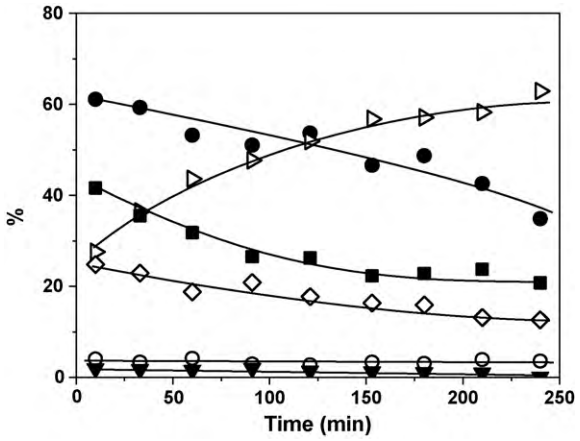

Fig. 8. Reactants: anisole/phenol mixture. Anisole conversion (●) and selectivities on HBEA. Selectivities to: phenol (▷), *o*-cresol (■), *p*-cresol (◊), MA (○), and *m*-cresol (▼) (473 K, 101.3 kPa, phenol/anisole = 5, $W/F^0_{anisole} = 27$ g h/mol).

anisole/phenol mixture is contacted with zeolites HZSM5 and HMCM22.

3.2.2.4. Reactants: anisole/methanol mixture. Finally, we fed to the reactor an anisole/methanol mixture and determined the zeolites activity and selectivity. Fig. 9 shows the results obtained on zeolite HMCM22. The activity decay on stream was significant on HMCM22 and the anisole conversion decreased from about 100% at $t = 0$ to 44% at the end of the run. Dymethylether (DME) and hydrocarbons were detected among the reaction products which suggests that the formation of coke via methanol dehydration and consecutive DME conversion to hydrocarbons (Reaction 8) may be responsible for the catalyst deactivation observed in Fig. 9. Reaction 8 has been widely investigated on solid acids [29] and it has been reported that the formation of hydrocarbons increases with the strength of

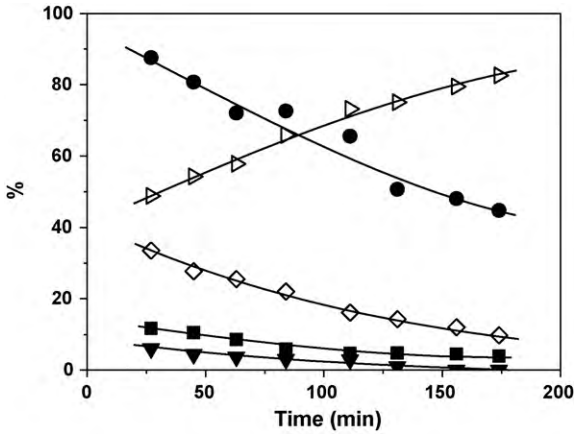

Fig. 9. Reactants: anisole/methanol mixture. Anisole conversion (●) and selectivities on HMCM22. Selectivities to: phenol (▷), *o*-cresol (■), *p*-cresol (◊), *m*-cresol (▼) (473 K, 101.3 kPa, methanol/anisole = 5, $W/F^0_{anisole} = 112$ g h/mol).

Brønsted acid sites [30]. Catalytic results obtained at $t = 0$ on HBEA, HZSM5 and HMCM22 are presented in Table 5. Zeolites HBEA and HZSM5 yielded mainly phenol that would be essentially formed by anisole dealkylation (Reaction 4). Nevertheless, formation of phenol via Reaction 9 cannot be excluded because of the high methanol/anisole molar ratio in the feed (methanol/anisole = 5).

Reaction 8: Methanol dehydration

$$2\,CH_3OH \longrightarrow H_2O + CH_3OCH_3 \longrightarrow \text{Hydrocarbons}$$

Methanol DME

In contrast with zeolites HBEA and HZSM5, HMCM22 formed significant amounts of *p*-cresol (Table 5). Fig. 9 shows that the selectivity to phenol increased with time on stream at the expense of *p*-cresol, thereby suggesting that *p*-cresol is formed from the consecutive methylation of phenol.

Reaction 9: Formation of phenol from anisole and methanol

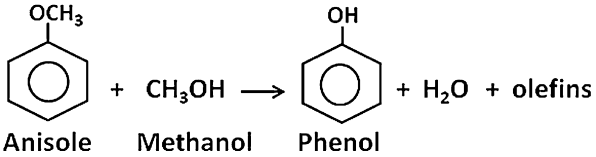

As already observed in Fig. 4, methylation of phenol on HMCM22 produces mainly *p*-cresol because its narrow pore structure hampers the formation of bulkier *o*-cresol isomer.

3.3. Reaction networks for phenol methylation

Based on our catalytic results detailed above and previous works [9,10] we postulated in Figs. 10–12 the reaction mechanism pathways of phenol methylation on zeolites HBEA, HZSM5 and HMCM22, respectively. Let us first analyze the phenol methylation mechanism on HBEA (Fig. 10). Phenol is alkylated to primary and secondary products without significant diffusional restraints on HBEA and the reaction proceeds yielding increased amounts of dialkylated products (xylenol isomers) as phenol conversion increases (Fig. 4). Phenol initially reacts with methanol via two parallel alkylation reactions: by *O*-alkylation phenol is transformed to anisole and by *C*-alkylation yields *o*- and *p*-cresols. *m*-Cresol isomer is not formed directly from phenol. Initially, HBEA forms similar amounts of anisole and *o*-cresol, and the *o*-cresol/*p*-cresol ratio is close to 2, corresponding to the statistic attack of the aromatic ring by methanol in *ortho* and *para* positions. *o*-Cresol is consecutively alkylated mainly to 2,4- and 2,6-xylenols (*C*-alkylation), but also forms minor amounts of 2-MA (*O*-alkylation) (Table 2). *o*-Cresol isomerization to *m*-cresol is not significant. In the reaction network of Fig. 10 we assumed that *p*-cresol is alkylated to the corresponding dialkyl isomers (2,4-xylenol and 4-MA) by similar reaction pathways than *o*-cresol (we did not perform catalytic runs using *p*-cresol as a reactant). Anisole may undergo several consecutive reactions, but under the operating conditions of phenol methylation (simultaneous presence of phenol and methanol) our results show that the most important anisole

Table 5
Catalytic results for anisole/methanol reactions.

Catalyst	$X_{anisole}$ at $t = 0$ (%)	Selectivity at $t = 0$ (%)					
		Phenol	*o*-Cresol	*m*-Cresol	*p*-Cresol	Xylenols	MA
HBEA	60	72	6	0	6	0	16
HZSM5	60	80	9	0	7	0	4
HMCM22	98	39	14	5	42	0	0

$T = 473$ K, $P = 101.3$ kPa, $P_{anisole} = 1.013$ kPa, and methanol/anisole = 5.

conversion pathways are the phenol/anisole reaction to yield *o*- and *p*-cresol isomers (Reaction 7, Table 4), anisole methylation to methylanisoles (Table 5) and anisole dealkylation to phenol and olefins (Reaction 4, Tables 3 and 4). Thus, anisole reaches a maximum concentration with increasing residence time (Fig. 4); for phenol conversion values higher than 80% anisole is detected only in trace amounts. Anisole disproportionation is not an important reaction and produces only minor amounts of MA (Reaction 3, Table 4). In Fig. 10 we also include the methanol dehydration pathway to DME that is consecutively converted to hydrocarbons.

The reaction network for methylation of phenol on HZSM5 is shown in Fig. 11. The density of surface acid sites on HZSM5 is higher than on HBEA, but the distribution of Lewis and Brønsted sites is similar on both zeolites (L/B ratio about 1). The observed differences in product distribution between HBEA and HZSM5 are essentially caused by diffusional constraints operating in HZSM5 that impede the formation of bulky intermediates leading to dialkylated compounds. Selectivities to primary products (anisole, *o*- and *p*-cresol) on HZSM5 are similar to those determined on HBEA. But the methylation rate of *o*-cresol to xylenols, in particular 2,6-xylenol, severely decreases on HZSM5 (Table 2). Regarding the anisole conversion reactions, the alkylation of phenol with anisole to yield cresol isomers is suppressed (Table 4) whereas the formation of MA from anisole methylation drastically diminishes (Table 5).

The product distribution of phenol methylation on HMCM22 is significantly different than those observed on HBEA and HZSM5 (Fig. 4). The particular pore structure of zeolite HMCM22 promotes the selective formation of *p*-cresol among the primary products and drastically suppresses the consecutive reactions forming secondary products. The reaction pathways for phenol methylation on HMCM22 are presented in Fig. 12. Zeolite HMCM22 has unique pore architecture with two independent pore systems. One pore system is tridimensional and composed of 12-member ring (MR) supercages (18.2 Å × 7.12 Å × 7.1 Å) connected by 10-MR windows (4.0 Å × 5.5 Å). The second, bidimensional, is composed of interconnected sinusoidal 10-MR channels (4.0 Å × 5.0 Å) and does not contain any cages [19,31]. The small pores of zeolite HMCM22 can change the product distribution of phenol methylation reaction according to the ease of diffusivity of product molecules. In fact, only molecules that can diffuse through the 10-MR pores of HMCM22 may reach the internal active sites of this zeolite because the 12-MR supercages are connected to the exterior through a 10-MR window. Difference of the transport rates of *p*- and *o*-

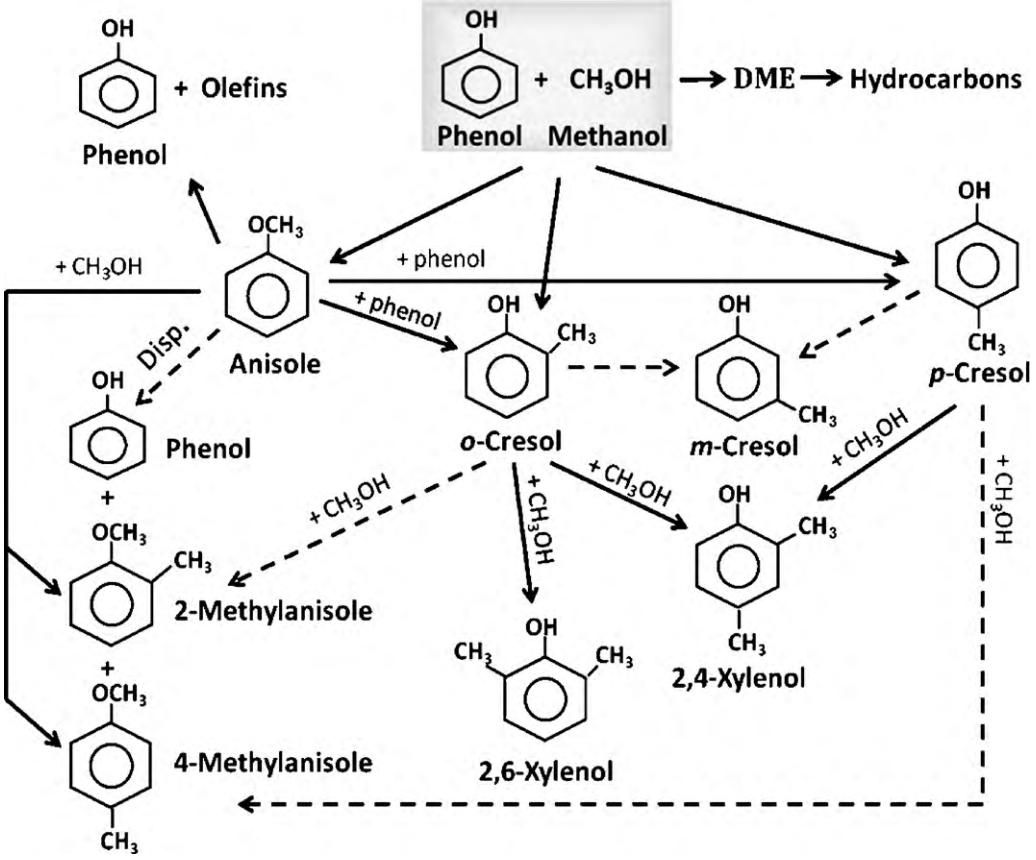

Fig. 10. Reaction kinetic network for phenol methylation on HBEA. Dotted lines indicate minor relevance of the reaction pathway.

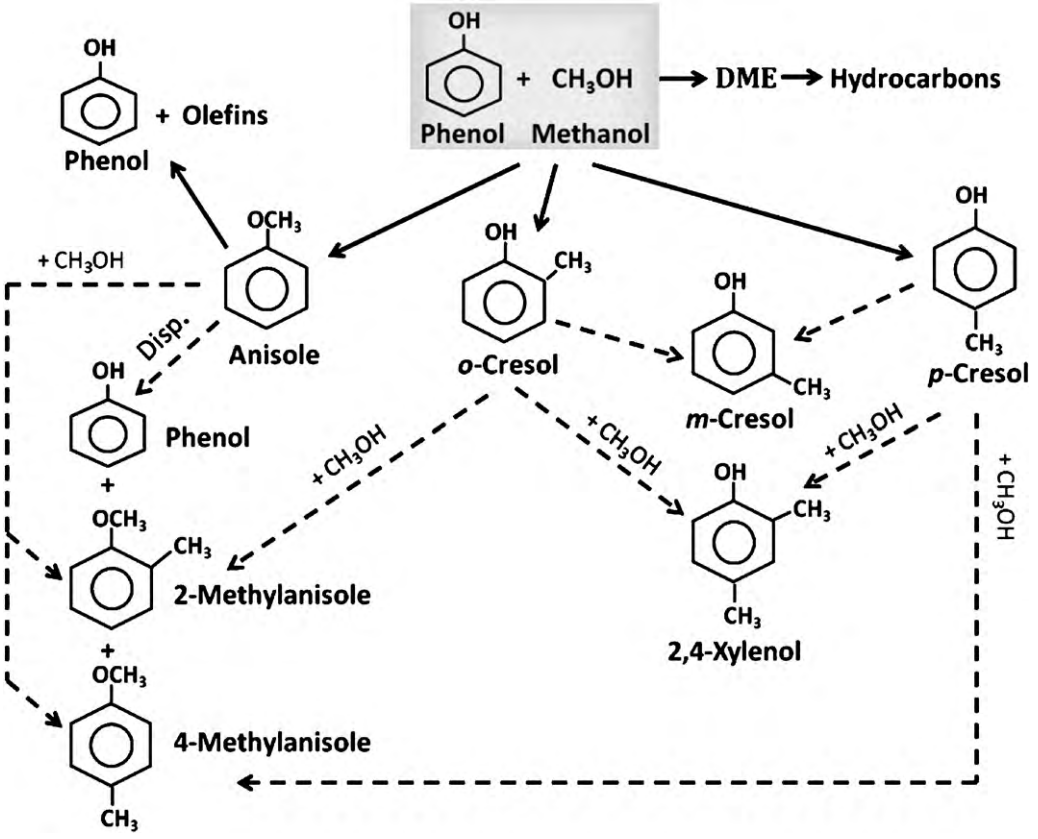

Fig. 11. Reaction kinetic network for phenol methylation on HZSM5. Dotted lines indicate minor relevance of the reaction pathway.

cresol isomers in the 10-MR pores of HMCM22 may explain the drastic *para*-selectivity improvement observed in this work for the gas-phase methylation of phenol on HMCM22 as compared to HZSM5 or HBEA. Our results on HMCM22 reveal that phenol can go inside the sinusoidal 10-MR channels and form cresol isomers but *o*-cresol would diffuse at much smaller rates than *p*-cresol. In a previous work [17], we calculated the initial formation rates of primary products (r_i^0) and observed that $r^0_{p\text{-cresol}}/r^0_{o\text{-cresol}}$ and $r^0_{p\text{-cresol}}/r^0_{\text{anisole}}$ ratios were about 0.7 and 0.6, respectively, on HBEA and HZSM5, but reached values of 4.1 and 7.7 on HMCM22. Thus, zeolite HMCM22 suppresses the formation of anisole and also significantly decreases the *o*-cresol formation rate, but yields *p*-cresol at high rates. Formation of secondary dialkylated compounds such as MA and xylenols were completely suppressed on HMCM22 (Fig. 4 and Tables 3 and 5). In contrast, isomerization reactions between monoalkylated products were promoted on HMCM22 (Tables 2 and 5) because of its high concentration of strong Brønsted acid sites. Thus, formation of *m*-cresol from con-

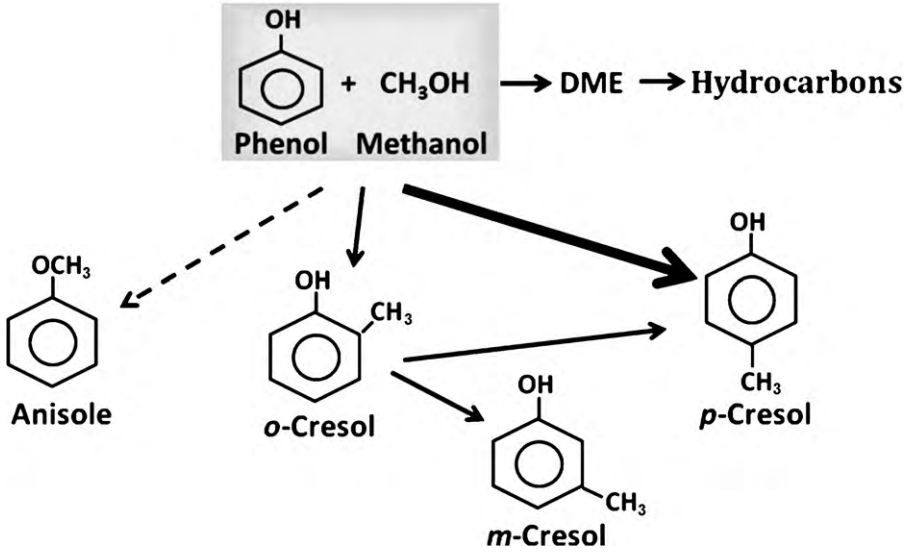

Fig. 12. Reaction kinetic network for phenol methylation on HMCM22. Dotted lines indicate minor relevance of the reaction pathway. The broad line indicates major relevance of the reaction pathway.

secutive isomerization of *o*-cresol reached about 12% at $X_P^0 \cong 95\%$ (Fig. 4). Finally, it must be noted that the activity decay on HMCM22 during the methylation of phenol was similar to that observed on HBEA, thereby suggesting that the reactions forming coke intermediates such as methanol dehydration are not suppressed to any significant extent on HMCM22.

4. Conclusions

The phenol methylation reaction mechanism on HBEA, HZSM5 and HMCM22 depend on the zeolite pore structure and acid properties. The three zeolites form the same primary products via *O*-alkylation (anisole) and *C*-alkylation (*o*- and *p*-cresol) of phenol. Secondary products are *m*-cresol, 2,4- and 2,6-xylenols, and 2- and 4-methylanisole. On HBEA, anisole reacts with phenol to yield *o*- and *p*-cresol isomers, or with methanol to give methylanisoles; anisole may be also dealkylated to phenol and olefins. Besides, zeolite HBEA alkylates *o*-cresol mainly to 2,4- and 2,6-xylenols and to a lesser extent to 2-methylanisole. In contrast, HBEA practically does not isomerize *o*-cresol to *m*-cresol. The phenol methylation reaction occurs on HBEA without significant diffusional constraints and thus phenol is increasingly alkylated to dialkylated products (xylenol isomers) as phenol conversion increases.

Initial selectivities to primary products on HZSM5 are comparable to those determined on HBEA, probably because the distribution of Lewis and Brønsted acid sites is similar on both zeolites. However, the product distribution is different on HZSM5 in comparison to HBEA because formation of bulky intermediates involved in the formation of secondary products is hampered by intracrystalline diffusion on HZSM5. Specifically, zeolite HZSM5 drastically decreases the rates of *o*- and *p*-cresol methylations to xylenols, anisole methylation to methylanisoles, and anisole/phenol alkylation to cresol isomers. Thus, for a given conversion of phenol, zeolite HZSM5 forms more anisole and less xylenols than HBEA.

The product distribution of phenol methylation on HMCM22 is significantly different than those observed on HBEA and HZSM5. The particular pore structure of zeolite HMCM22 promotes by shape selectivity the formation of *p*-cresol at the expense of anisole and *o*-cresol among the primary products. Besides, the narrow channels of zeolite HMCM22 completely suppress the formation of secondary dialkylated compounds such as methylanisoles and xylenols. On the other hand, formation of *m*- and *p*-cresol from consecutive *o*-cresol isomerization is improved on HMCM22 because of its high concentration of strong Brønsted acid sites. Thus, zeolite HMCM22 is a highly suitable catalyst for selectively promoting the reaction pathways forming *p*-cresol in the phenol methylation reaction mechanism.

Acknowledgements

We thank the Universidad Nacional del Litoral (UNL), the Agencia Nacional de Promoción Científica y Tecnológica (ANPCyT) and the Consejo Nacional de Investigaciones Científicas y Técnicas (CONICET), Argentina, for the financial support of this work.

References

[1] J.E. Bailey, M. Bohnet, J. Brinker (Eds.), Ullman's Encyclopedia of Industrial Chemistry, 6th ed., Willey–VCH, Weinheim, 1988.
[2] B.M. Devassy, G.V. Shanbhag, F. Lefebvre, S.B. Halligudi, J. Mol. Catal. A: Chem. 210 (2004) 125.
[3] G.L. Gregory, General Electric Co., US Patent 4,933,509 (1989).
[4] K. Tanabe, W.F. Hölderich, Appl. Catal. A: Gen. 181 (1999) 399.
[5] S. Velu, C.S. Swamy, Appl. Catal. A: Gen. 119 (1994) 241.
[6] S. Balsama, P. Beltrame, P.L. Beltrame, P. Carniti, L. Forni, G. Zuretti, Appl. Catal. 13 (1984) 161.
[7] M. Renaud, P. Chantal, S. Kaliaguine, Can. J. Chem. Eng. 64 (1986) 787.
[8] M. Marczewski, G. Perot, M. Guisnet, in: M. Guisnet, J. Barrault, C. Bouchoule, D. Duprez, C. Montassier, G. Pérot (Eds.), Studies in Surface Science and Catalysis, 41, Elsevier, Amsterdam, 1988, p. 273.
[9] M. Marczewski, J.P. Bodibo, G. Perot, M. Guisnet, J. Mol. Catal. 50 (1989) 211.
[10] E. Santacesaria, D. Grasso, D. Gelosa, S. Carrá, Appl. Catal. 64 (1990) 83.
[11] K. Tanabe, T. Nishizaki, in: G.C. Bond, P.B. Wells, F.C. Tompkins (Eds.), Proc. 6th Int. Congr. Catal., vol. 2, The Chemical Society, London, 1977, p. 863.
[12] M. Bregolato, V. Bolis, C. Busco, P. Ugliengo, S. Bordiga, F. Cavani, N. Ballarini, L. Maselli, S. Passeri, I. Rossetti, L. Forni, J. Catal. 245 (2007) 283.
[13] M.E. Sad, C.L. Padró, C.R. Apesteguía, Catal. Today 133–135 (2008) 720.
[14] K.G. Bhattacharyya, A.K. Talukdar, P. Das, S. Sivasanker, J. Mol. Catal. 197 (2003) 255.
[15] P. Beltrame, P.L. Beltrame, P. Carniti, A. Castelli, L. Forni, Appl. Catal. 29 (1987) 327.
[16] G. Moon, W. Böhringer, C.T. O'Connor, Catal. Today 97 (2004) 291.
[17] M.E. Sad, C.L. Padró, C.R. Apesteguía, Appl. Catal. A: Gen. 342 (2008) 40.
[18] M.K. Rubin, P. Chu, US Patent 4,954,325 (1990).
[19] S.L. Lawton, A.S. Fung, G.J. Kennedy, L.B. Alemany, C.D. Chang, G.H. Hatzikos, D.N. Lissy, M.K. Rubin, H.K.C. Timken, S. Steuernagel, D.E. Woesner, J. Phys. Chem. 100 (1996) 3788.
[20] Y. Miyamoto, N. Katada, M. Niwa, Micropor. Mesopor. Mater. 40 (2000) 271.
[21] E.P. Parry, J. Catal. 2 (1963) 371.
[22] J.W. Ward, J. Catal. 10 (1968) 34.
[23] H. Knözinger, Adv. Catal. 25 (1976) 184.
[24] J. Wang, L. Huang, H. Chen, Q. Li, Catal. Lett. 55 (1998) 157.
[25] D. Meloni, S. Laforge, D. Martin, M. Guisnet, E. Rombi, V. Solinas, Appl. Catal. A: Gen. 215 (2001) 55.
[26] A. Corma, C. Corell, V. Fornés, W. Kolodziejski, J. Pérez-Pariente, Zeolites 15 (1995) 576.
[27] J.M. Jacobs, R.F. Parton, A.M. Boden, P.A. Jacobs, in: M. Guisnet, J. Barrault, C. Bouchoule, D. Duprez, C. Montassier, G. Pérot (Eds.), Studies in Surface Science and Catalysis, vol. 41, Elsevier, Amsterdam, 1988, p. 221.
[28] J. Kaspi, G.A. Olah, J. Org. Chem. 43 (1978) 3142.
[29] M. Stöcker, Micropor. Mesopor. Mater. 29 (1999) 3.
[30] T. Tsoncheva, R. Dimitrova, Appl. Catal. A: Gen. 225 (2002) 101.
[31] M.E. Leonowicz, J.A. Lawton, S.L. Lawton, M.K. Rubin, Science 264 (1994) 1910.